Desalination and Water Treatment
www.deswater.com

doi: 10.5004/dwt.2023.29171

282 (2023) 220–236
January

Pine needle biochar loaded with iron–nickel bimetal composite as heterogeneous catalysts to activate peroxymonosulfate for efficient degradation of oxytetracycline

Yan Chen, Mingyi Liu, Wenwen Fan, Pengfei Xiao*

College of Forestry, Northeast Forestry University, Harbin 150040, China, email: xpfawd@nefu.edu.cn (P. Xiao)
ORCID: 0000-0002-0379-4358, emails: 1992831456@qq.com (Y. Chen), 1711335104@qq.com (M. Liu), 2952623984@qq.com (W. Fan)

Received 19 August 2022; Accepted 1 December 2023

ABSTRACT

Residual antibiotics in the environment pose a serious threat to the environment. To solve the problems of inter-particle agglomeration, metal ion leaching and difficult recovery of transition metal oxides as catalysis in advanced oxidation processes for the treatment of antibiotic wastewater, pine needle biochar loaded with iron–nickel bimetals (Fe/Ni@PNBC) were successfully produced by the impregnation–co-precipitation method to activate peroxymonosulfate (PMS) for degradation of oxytetracycline (OTC). The Fe/Ni@PNBC catalyst has good surface properties, abundant functional groups and catalytic stability. Under the optimal conditions, the degradation efficiency of OTC with initial concentration of 10~60 mg/L is close to 90%. In addition, $^1O_2$ and $O_2^{\bullet-}$ played a major role in OTC degradation. The reaction mechanism for generation of active species and OTC degradation in the reaction system was proposed from two perspectives including redox of iron and nickel ions in different valence states and interconversion between the active substances. After 5 cycles, Fe/Ni@PNBC still maintained a high catalytic activity for OTC degradation. This study provides a new method to prepare an economical and environmentally friendly catalyst for activating PMS to treat antibiotic wastewater.

Keywords: Oxytetracycline; Peroxymonosulfate; Heterogeneous catalyst; Reactive oxygen species; Reaction mechanism; Oxidative degradation

1. Introduction

Oxytetracycline (OTC) is extensively used in medicine and animal husbandry as one of the broad-spectrum antibiotics [1]. However, OTC is released into the environment without being fully used, which has led to the widespread presence of OTC residues in the environment and caused a significant risk to human and aquatic wildlife [2]. Meanwhile, wastewater treatment plants cannot effectively remove antibiotics using biotechnology due to most antibiotics are less biodegradable [3]. Therefore, it is particularly important to develop processes for the efficient reduction of OTC and its derivatives.

In order to effectively degrade antibiotics in the environment, predecessors have used physical, biological and chemical methods among which advanced oxidation processes (AOPs) have been extensively researched [4–6]. AOPs based on highly reactive radicals have the ability to degrade antibiotics into less toxic substances. The highly reactive radicals involved in the reaction include hydroxyl radicals ($^{\bullet}OH$), sulfate radicals ($SO_4^{\bullet-}$) and superoxide radicals ($O_2^{\bullet-}$) [7]. In previous studies, researchers have constructed AOPs by using ozone (O_3) [8], hydrogen peroxide (H_2O_2), UV light and ultrasound and so forth [9]. Among them, compared to other oxidation methods, the oxidation process based on persulfate exhibits

* Corresponding author.

longer half time, greater selectivity, acidity range adaptation, as well as higher redox potential ($SO_4^{\bullet-}$, E^0 = 2.5–3.1 V) [10,11]. Therefore, $SO_4^{\bullet-}$-AOPs are widely used to treat organic wastewater. According to the research results, peroxymonosulfate (PMS, HSO_5^-) can generate surface radicals through thermal activation, transition metal, UV and ultrasonic activation [12,13]. Although these methods are effective in activating PMS, they suffer from high costs, secondary pollution from heavy metal leaching and high energy consumption [14,15]. As a result, the exploitation of an environmentally friendly and economical catalyst is of great importance.

New carbonaceous materials, represented by biochar, are widely used in the field of environmental remediation thanks to their low economic cost, environmental friendliness, high adsorption capacity, wide range of sources and simplicity of preparation [16]. Metals are also very hotly researched in the direction of catalyzing persulfate, such as iron, nickel, cobalt, copper and so on. Studies have shown that iron–nickel composites exhibit synergistic effects in the persulfate system, which can effectively degrade organic matter in groundwater [17]. However, the use of metallic materials alone suffers from problems such as secondary contamination of water bodies due to the leaching of metal ions and the agglomeration of catalytic materials [18]. Therefore, this project combines biochar and bimetal to give full play to the stability of biochar and the synergistic function of iron–nickel bimetal activating PMS, making up for the shortcomings of physical adsorption of biochar and catalysis of using metal alone and optimizing the performance of catalyst, the researchers constructed biochar-based metal non-homogeneous catalytic materials.

Consequently, in this research, pine needle biochar (PNBC) with large specific surface area, abundant pores and structural defects was prepared by high temperature pyrolysis using pine needle as raw biomass material, and Fe–Ni bimetal supported PNBC (Fe/Ni@PNBC) was prepared by impregnation–co-precipitation process, which was utilized to activate PMS for the degradation of OTC as a heterogeneous catalyst. The main purpose of this study involved (1) investigating the optimum Fe/Ni molar ratio in the prepared catalysts with maximum catalytic capacity; (2) analyzing the physical properties and chemical composition of catalysts using a variety of characterization methods; (3) exploring the optimal process parameters for OTC degradation in Fe/Ni@PNBC/PMS systems; (4) resolving the activation mechanism of PMS by Fe/Ni@PNBC catalyst; (5) verifying the catalytic stability and reusability of Fe/Ni@PNBC.

2. Materials and methods

2.1. Reagents

Oxytetracycline ($C_{22}H_{24}O_9N_2{\cdot}2H_2O$, 97%), potassium monopersulfate ($KHSO_5{\cdot}0.5KHSO_4{\cdot}0.5K_2SO_4$, >42% $KHSO_5$ basis), nickel chloride hexahydrate ($NiCl_2{\cdot}6H_2O$, 99.9%), iron nitrate nonahydrate ($Fe(NO_3)_3{\cdot}9H_2O$, AR, 99%), sodium hydroxide (NaOH, 96%), sodium hydrogen carbonate ($NaHCO_3$, 99.5%), potassium nitrate (KNO_3, 99%), potassium phosphate monobasic (KH_2PO_4, 99.5%), sodium chloride (NaCl, 99.5%), sodium carbonate anhydrous (Na_2CO_3, 99.8%), ethanol (EtOH, AR, >99.5%), methanol (MeOH, AR, 99.5%), p-benzoquinone (p-BQ, 99%), tert-butyl alcohol (TBA, GR, >99.5%), furfuryl alcohol (FFA, CP, 97%) and humic acid (HA, FA > 90%) were purchased from Shanghai Aladdin Corporation. Throughout the experiment, all the reagents used were of analytical grade, and the ultrapure water was used for dissolution and dilution.

2.2. Preparation of Fe/Ni@PNBC

PNBC was prepared from pine needles (*Pinus tabulaeformis*) collected from the campus of Northeast Forestry University. After repeatedly cleaning with ultrapure water, clean pine needles were dried in a 60°C oven. Then, the dried pine needles were roasted for 3 h in a muffle furnace at 500°C and passed through a 120-mesh sieve after being ground in a mortar. To remove the pyrolysis ash, the biochar was rinsed with ultrapure water. After drying for 24 h at 60°C, it was placed in a brown sample bottle.

The catalyst was prepared by impregnation–co-precipitation with PNBC as raw material. First, using a magnetic stirrer, 0.2 g biochar was thoroughly disseminated in 30 mL ultrapure water. Then, 0.04 mol/L $Fe(NO_3)_3{\cdot}9H_2O$ and an amount of $NiCl_2{\cdot}6H_2O$ were dissolved in 10 mL ultrapure water and then added into the above solution. It should be noted that catalysts with Fe/Ni molar ratios of 1:1, 2:1 and 3:1 were obtained by keeping the amount of $Fe(NO_3)_3{\cdot}9H_2O$ and changing the amount of Ni to 0.04, 0.02 and 0.013 mol/L, respectively. After being stirred evenly, the materials were soaked for 0.5 h. Then 0.4 mol/L NaOH was added to the mixed solution at a constant rate until the pH value reached 10–11 and the tan precipitate was produced. After the precipitation was complete, the mixture was agitated for 1 h at 80°C, after which the precipitate was detached and rinsed with ultrapure water until the pH value was neutral. It was then dried overnight at 60°C and kept in a brown glass bottle until needed. Fe–Ni materials supported by PNBC with load ratios of 1:1, 2:1 and 3:1 were prepared and named Fe/Ni1@PNBC, Fe/Ni2@PNBC and Fe/Ni3@PNBC, respectively.

2.3. Experimental procedures

All degradation experiments were performed in a 250 mL conical flask. At room temperature, 50 mL PMS solution and 50 mL OTC solution were added to the reactor, followed by rapid addition of Fe/Ni@PNBC, capping and placing the reactor in a thermostatic air shaker. At a specific time interval, a syringe was used to retrieve 3.0 mL of supernatant and injected it into a colorimeter through a 0.45 μm filter. The OTC residual concentration was immediately measured at 355 nm with a UV-Vis spectrophotometer to evaluate the catalytic effect of the catalyst. The adsorption tests were performed under the same conditions except that there was no PMS solution.

Moreover, a number of experiments by controlling with a single variable were conducted in order to acquire the ideal degradation conditions, including the load Fe–Ni ratio (1:1, 2:1 and 3:1), catalyst dosage (0.5, 1.0, 1.5 and 2.0 g/L), PMS concentration (0.5, 1.0, 1.5, 2.0 and 2.5 g/L), initial OTC concentration (10, 20, 40, 60 and 80 mg/L), and initial pH

value (5.0, 7.0, 9.0 and 11.0). In the influence experiment of coexistence anions (Cl^-, HCO_3^-, CO_3^{2-}, NO_3^- and $H_2PO_4^-$), three gradients (20, 40 and 60 mmol/L) were set for each ion. To explore the effect of organic matter on degradation, HA (5, 10 and 20 mg/L) was added to the reactor. In the free radical quenching experiments, TBA was utilized to quench OH, p-BQ and FFA were used to quench $O_2^{\bullet-}$ and $^1O_2$, respectively, while the purpose of using EtOH was used to quench $SO_4^{\bullet-}$ and OH. For the catalyst cycling experiments, the used catalyst was fully cleaned three times with ultrapure water, then dried at 60°C for 4 h and repeated the experiment according to the above process to estimate the stability and reusability of the catalyst. All of the preceding experiments were repeated three times in a row, with the average findings utilized to process the data.

2.4. Analytical methods

The OTC concentration was measured by a TU-1901 ultraviolet spectrophotometer (PGENERAL, China) at 355 nm, based on the standard curve of absorbance and concentration (Fig. S1). The pH of the solution was determined using a FE20 Precision pH meter (Mettler Toledo, Zurich, Switzerland). The morphology and microstructure of Fe/Ni1@PNBC before and after reaction were analyzed by using a SU8020 scanning electron microscope (SEM, Hitachi, Japan). ASAP 2460 physical adsorption analyzer (Micromeritics, China) was used to determine the specific surface area and porosity of PNBC and catalyst. The loaded X-ray diffraction patterns for each Fe–Ni ratio were obtained by X-ray diffractometer (XRD, TD-3500, Tongda) and phase composition was determined. The elemental composition and valence state before and after reaction were analyzed by ESCALAB 250 Xi X-ray photoelectron spectroscopy (XPS, Thermo Fisher, America). The functional groups of the catalyst were analyzed by iS10 FTIR Spectrometer (FTIR, Nicolet, US). Electron paramagnetic resonance spectra were attained with an A300-10/12 electron paramagnetic resonance spectrometer (EPR, Bruker, Germany) to capture free radicals produced by the Fe/Ni1@PNBC/PMS system. The total organic carbon (TOC) was measured by a TOC-LCPN analyzer (Shimadzu, Japan). A thermogravimetric analyzer (TG, NETZSCH, Germany) was used to evaluate the thermal stability of Fe/Ni1@PNBC.

3. Results and discussion

3.1. Effect of Fe–Ni ratio on the removal of OTC

In the experiment, investigating the adsorption and degradation capacity of OTC by prepared materials with different Fe–Ni ratios when the initial OTC concentration was 80 mg/L, the PMS concentration was 2.0 g/L, and the catalyst dosage was 2.0 g/L. According to Fig. 1a, the adsorption rate of OTC by PNBC was as high as about 60%, while when the Fe–Ni metals were loaded in PNBC, the adsorption rate of OTC decreased significantly. The adsorption rate of Fe/Ni1@PNBC to OTC was 19%, which was close to that of Fe/Ni2@PNBC (20%), while that of Fe/Ni3@PNBC was 38%, after 60 min. The adsorption efficiency of Fe/Ni@PNBC to OTC increased with the increase of Fe/Ni ratio. The possible mechanism is that the adsorption sites exposed on the surface of PNBC increased with the decrease of Ni^{2+} content, so the adsorption rate increased. It has been reported that iron ions can form stable complexes with OTC [19], and the reduction of Ni^{2+} content may lead to the increase of Fe^{3+} content in biochar pores, which form complexes with OTC and increased adsorption capacity.

The OTC degradation effect of the PMS system without catalyst was poor (about 40%), as shown in Fig. 1b. Moreover, the degradation efficiency of OTC was significantly improved after adding the catalysts, that is, Fe/Ni1@PNBC/PMS system had the best OTC removal effect and the highest reaction rate. The main reaction of PMS with the Fe–Ni redox cycle has been reported to form reactive oxygen species (ROS) such as $SO_4^{\bullet-}$, and the degradation of OTC is mainly based on ROS [5]. Therefore, the possible mechanism was that the amount of ROS generated by the reaction system decreased with the decrease of nickel ion content, leading to the decrease of degradation rate. It was noteworthy that the catalyst Fe/Ni1@PNBC had the lowest adsorption rate to OTC and the highest removal efficiency. According to these results, Fe/Ni1@PNBC was selected as the experimental catalyst, and its structural characteristic was further characterized to discuss the activation mechanism of PMS.

3.2. Characterization of Fe/Ni1@PNBC

The microstructure of the catalyst was observed using scanning electron microscopy (SEM). As indicated in Fig. 2a and b, the morphology of the catalyst is irregularly granular with the pore structure. At the same time, the large specific surface area and layered pore size of PNBC can promote the uniform distribution of metals on the surface of PNBC, and reduce the agglomeration of metal attached to PNBC, which generates more active sites and helps to activate PMS, thus effectively removing contaminants [20]. The morphological image of the reacted catalyst is shown in Fig. 2c and d. It can be observed that the metal particles are more uniformly distributed and the agglomeration phenomenon is reduced, indicating that the catalyst has excellent morphological characteristics and catalytic stability.

The Brunauer–Emmett–Teller (BET) specific surface area, total pore volume and average pore diameter of PNBC and Fe/Ni1@PNBC (before and after the reaction) were analyzed and the results are shown in Table 1. When the PNBC was loaded with Fe and Ni, its BET specific surface area increased significantly from 193.6327 to 241.2181 m^2/g. The *t*-plot external surface area increased from 55.1104 to 268.1128 m^2/g. The average pore diameter increased from 2.53229 to 2.89952 nm, while the total pore volume from 0.122583 to 0.174854 cm^3/g. These results indicate that both the surface structure and physical properties of the catalyst were changed during the preparation of the catalyst, so that the catalysts exhibited a large specific surface area. However, in previous adsorption experiments, the adsorption capacity of Fe/Ni@PNBC for OTC instead decreased, and the possible reason are that the adsorption performance is not only related to the specific surface area and pore size, but also related to the molecular

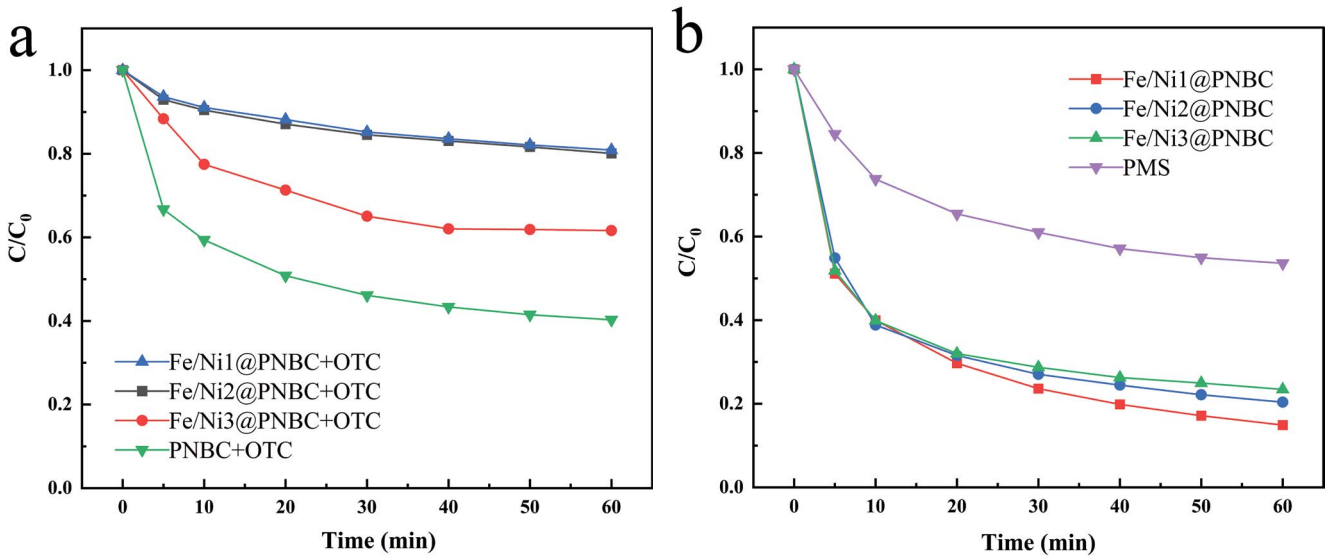

Fig. 1. Adsorption (a) and degradation (b) of OTC in different treatment systems, where Fe/Ni1, Fe/Ni2 and Fe/Ni3 mean that the molar ratio of Fe/Ni in the catalyst is 1:1, 2:1 and 3:1.

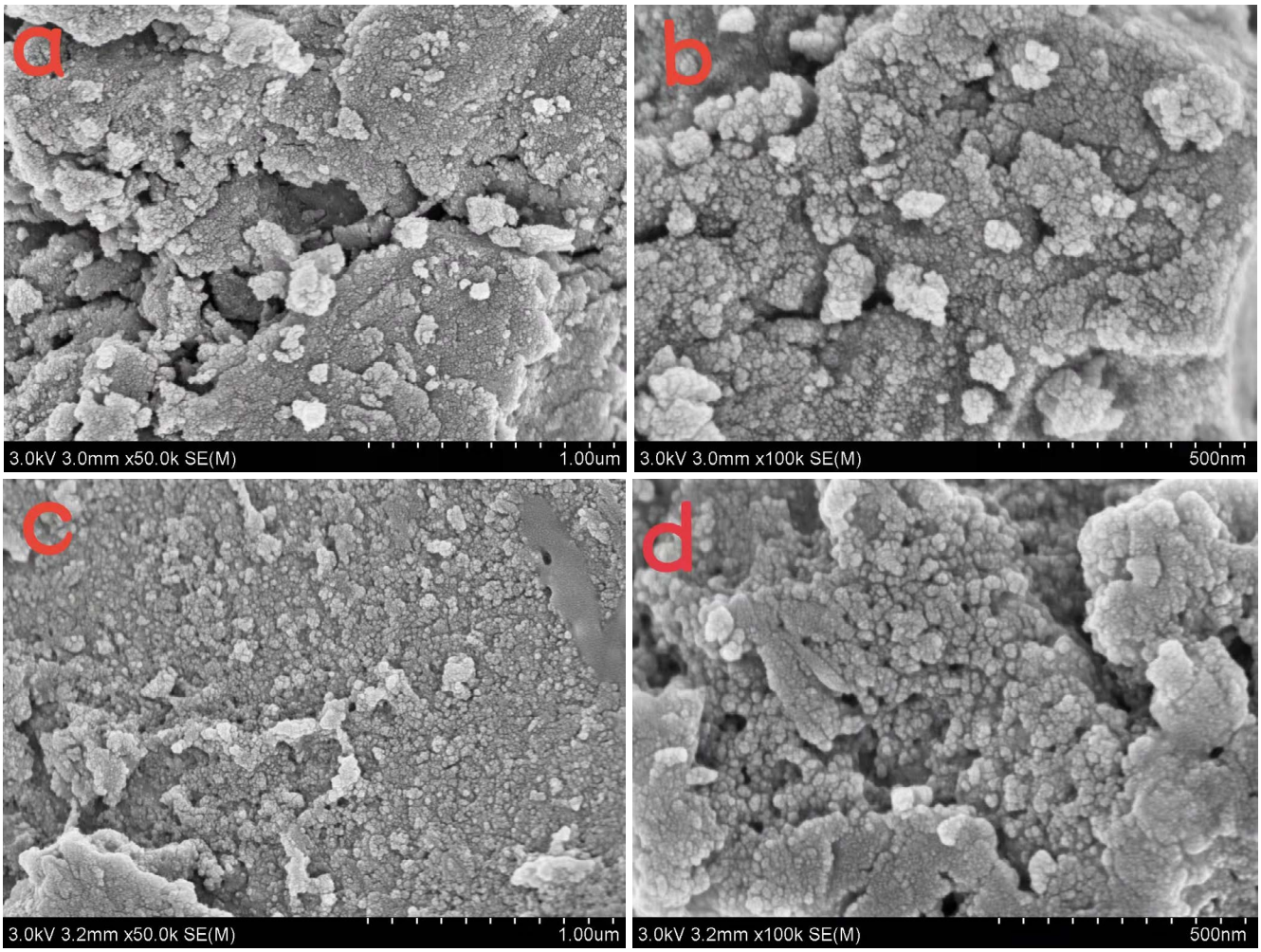

Fig. 2. SEM images of Fe/Ni1@PNBC before (a, b) and after (c, d) the reaction.

Table 1
Surface structure characterization of PNBC and Fe/Ni1@PNBC

Material	BET surface area (m^2/g)	*t*-Plot external surface area (m^2/g)	Total pore volume of pores (cm^3/g)	Average pore diameter (nm)
PNBC	193.6327	55.1104	0.122583	2.53229
Fresh Fe/Ni1@PNBC	241.2181	268.1128	0.174854	2.89952
Used Fe/Ni1@PNBC	192.2796	189.1435	0.136581	2.84130

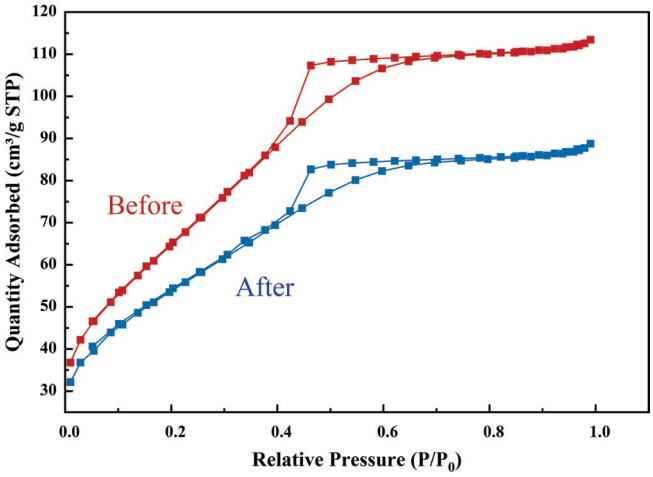

Fig. 3. Adsorption isotherms of Fe/Ni1@PNBC before and after reaction.

structure of the organic pollutants, and the aromaticity, polarity and stability of the adsorbent and other factors [21]. What is more, based on the comparison of the catalysts before and after the reaction, it is not difficult to find that there is a slight decrease in the *t*-plot external surface area and total pore volume of pores. Combined with the SEM images of the materials, we speculate that this phenomenon is due to the uniform distribution of metals on the catalyst after the reaction. All in all, the pore characteristics and specific surface area properties of the catalysts are relatively stable. Moreover, combined with Fig. 3, the adsorption isotherms of the catalysts before and after the reaction conform to the IUPAC IV-type isotherm and hysteresis loop H_2-type, which exhibits the adsorption characteristics of a mesoporous material.

Exploring the elemental composition of the Fe/Ni1@PNBC before and after a reaction by using XPS. And through using XRD to explore the phase composition of the catalyst before and after the reaction. Fig. 4a shows that the catalyst contains elements C, Fe, Ni and O, indicating that Fe and Ni were successfully loaded onto PNBC. Fig. 4b shows the high-resolution C1s spectra of used and fresh catalyst, and the spectra can be divided into three peaks at 284.8, 286.4 and 289.0 eV, independently, attributed to the functional groups C–C, C–OH, COOH of PNBC [22]. The high-resolution O1s spectra of fresh catalyst is divided into two peaks at 529.9 and 531.5 eV (Fig. 4c), which puts down to the formation of metal oxygen bond and the surface O–H group, respectively [23,24].

To investigate the valence state of the metal elements in the Fe/Ni1@PNBC, peak fits were made for Fe and Ni separately. The results showed that the fresh and used catalysts contained Fe(III), Fe(II) and Ni(II). The peak at 710.3 eV matched Fe(II), while the peaks at 711.7 and 714.7 eV matched Fe(III) [22] (Fig. 4d). The fresh catalyst contained 27.64% of Fe(II) and 72.36% of Fe(III). After the reaction, the Fe(II) content and the Fe(III) content decreased and increased by 4.81%. The Ni2p spectrum (Fig. 4e) exhibits a pair of intense spin-orbit doublets and satellite peaks. A pair of intense spin-orbit doublets of fresh catalyst at 856.1 and 873.5 eV were correlated with the characteristic peak of Ni2p3/2 and Ni2p1/2, which indicated that Ni(II) was located in the catalyst [25]. Meanwhile, comparing the spectrum of the Ni2p before and after the reaction, the content of Ni(II) was found to decrease by 2.06%. All in all, Fe(III), Fe(II), Ni(II) all were involved in activating PMS depending on the change in the content, while between Fe(III) and Fe(II), there were redox cycles.

As in Fig. 5a, Fe/Ni1@PNBC before the reaction displays characteristic peaks of $Ni(OH)_2{\cdot}0.75H_2O$ (PDF#38-0715). The diffraction peaks at 2θ = 11.35°, 22.74°, 33.46°, 33.40°, 38.77°, 45.98°, 59.98° and 61.25° corresponds to (003), (006), (101), (012), (015), (018), (110), (113) reflection of $Ni(OH)_2{\cdot}0.75H_2O$. Meanwhile, the FeO(OH) (PDF#75-1594) and $Fe_2O_3{\cdot}H_2O$ (PDF#08-0093) match the XRD pattern of the fresh Fe/Ni1@PNBC. Obviously, the results of the XRD analyses match those of the XPS analyses. Fe(III), Fe(II) and Ni(II) were loaded onto the catalyst. By comparing the patterns of Fe/Ni1@PNBC before and after the reaction (Fig. 5b), Fe/Ni2@PNBC and Fe/Ni3@PNBC, it is not difficult to find that the intensity of the peaks has become less, which is probably because the nickel content is relatively low. Therefore, nickel has an important role in activating PMS. It was noteworthy that there was no significant change in the XPS full spectrum of the catalyst before and after the reaction, and the intensity of the peaks between fresh Fe/Ni1@PNBC and used Fe/Ni1@PNBC didn't change significantly, which indicated the stability of the Fe/Ni1@PNBC.

Functional groups on catalyst surfaces were researched using Fourier-transform infrared spectroscopy (FTIR) analysis. By comparing the FTIR spectra (Fig. 5c) before and after the reaction, there was a little difference in the position of the vibration peaks, which advised that the reactive groups were almost identical. The vibration peak at 3,423.46 cm^{-1} was attributed to –OH stretching which possibly is ascribed to interlayer crystal water in the catalyst or hydroxyl groups in the PNBC [26]. The band of C–O stretching vibration was observed at 1,625 cm^{-1} around [27]. From the FTIR spectrum of the catalyst after the reaction,

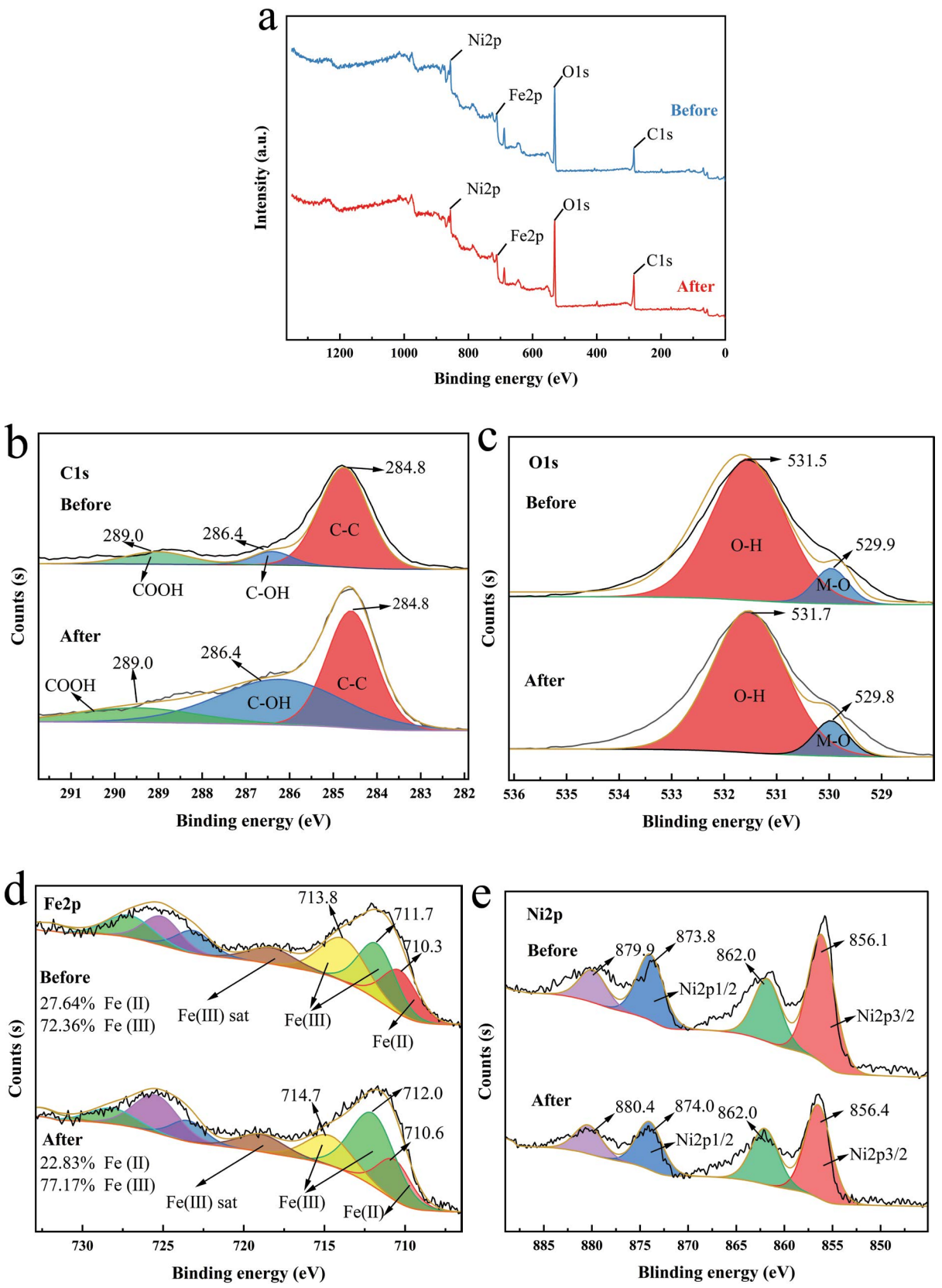

Fig. 4. XPS survey spectra (a) and high-resolution spectra of C1s (b), O1s (c), Fe2p (d) and Ni2p (e) of Fe/Ni1@PNBC before and after reaction.

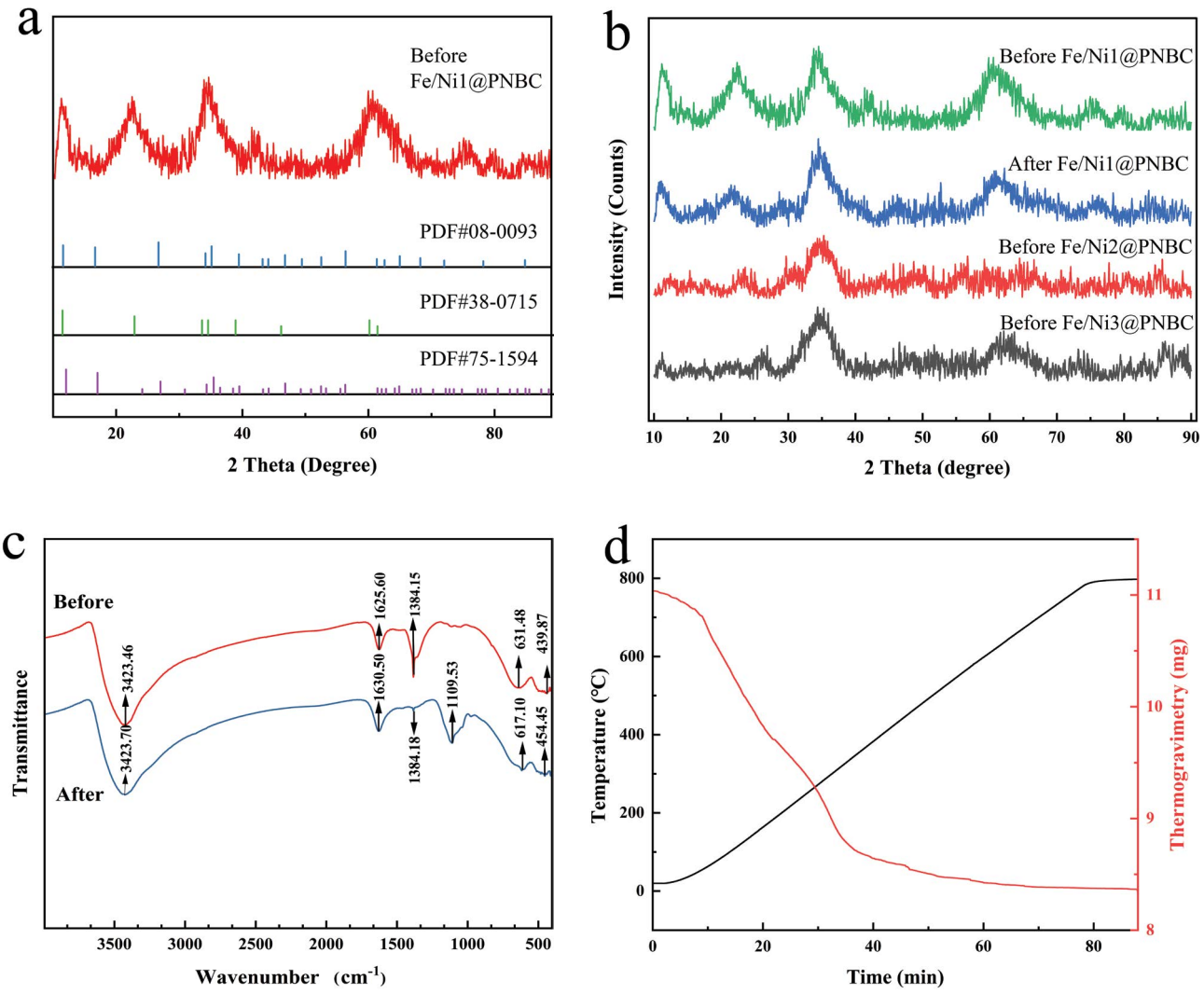

Fig. 5. XRD physical phase analysis of Fe/Ni1@PNBC (a), XRD patterns of Fe/Ni1@PNBC, Fe/Ni2@PNBC and Fe/Ni3@PNBC (b), FTIR spectra of Fe/Ni1@PNBC (c), and TG curve of Fe/Ni1@PNBC (d).

a vibration peak of 1,109 cm^{-1} was discovered, which was linked to the stretching vibration of S–O of SO_4^{2-}, indicating that the PMS was decomposed on the catalyst surface during the reaction and also indicated that the catalyst possessed the function of activating the PMS [28]. The vibrational peaks that appeared around 1,384 cm^{-1} were related to the C=O of the carboxylic group [27]. By comparing the intensity of the peaks before and after the reaction, it was found that the intensity of the peaks greatly reduced after the reaction, presumably due to the release of the proton from the COOH in PNBC, which activated the PMS in solution [22]. The stretching vibration of Fe–O–Fe is relevant for the bands at 631.48 and 617.10 cm^{-1} [29]. Meanwhile, the peaks at 439.87 and 454.45 cm^{-1} were related to ferrite characteristic of octahedral metal stretching in the low-frequency band [30].

The TG curve of Fe/Ni1@PNBC was shown in Fig. 5d. As can be seen from the figure, the mass loss of samples below 100°C was about 2.18%, which was regarded to be the removal of physical adsorption water [31]. When the temperature continued to rise, two steps of weightlessness appeared on the corresponding TG curve. The first step of weightlessness was due to the loss of crystal water, and the second-step was the removal of hydroxyl and carbonate ions in the form of H_2O and CO_2, respectively [32,33]. At about 400°C, the weight of the catalyst tended to be stable, and the total mass loss of the catalyst was about 23.6% when the heat treatment temperature was increased from room temperature to 800°C, showing excellent thermal stability.

3.3. Effect of experimental conditions on removal of OTC in Fe/Ni1@PNBC/PMS system

3.3.1. Initial concentration of OTC

The effects of different OTC concentrations on the system are shown in Fig. 6a (the catalyst dosage was 1.0 g/L, the PMS concentration was 1.0 g/L and without pH adjustment). When the initial concentration of OTC was 10 mg/L, the degradation rate was slower than that of other initial

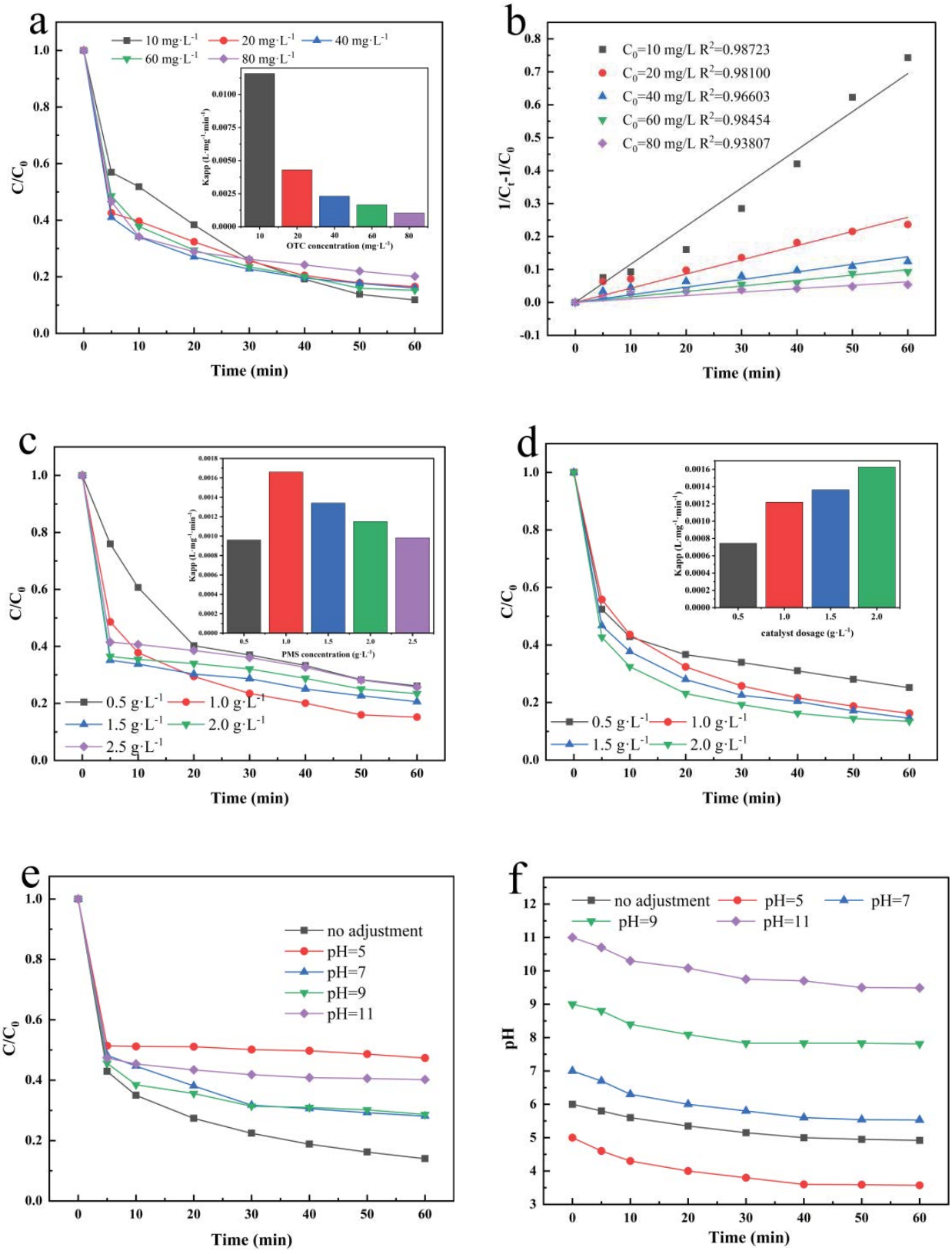

Fig. 6. Degradation rate of OTC at different initial concentrations (a), the kinetic curves of OTC degradation (b), the effect of the PMS concentration (c), catalyst dosage (d), initial solution pH (e) on the OTC degradation, and pH changes of reaction solutions at different initial pH values (f) in the Fe/Ni1@PNBC/PMS system, and the degradation of OTC under different air atmospheres.

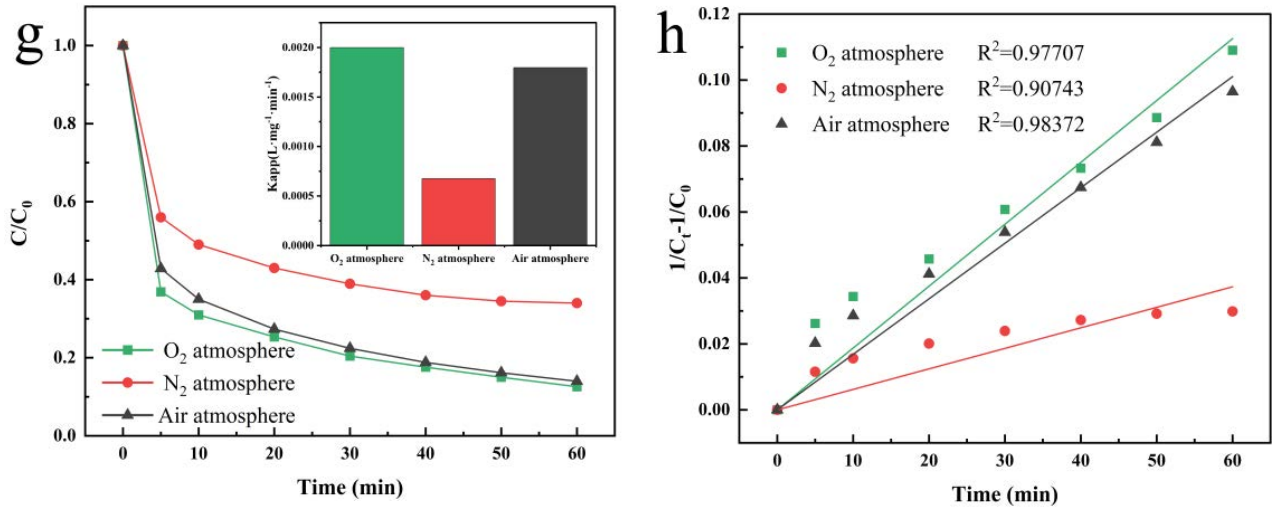

Fig. 6. (g) and its pseudo-second-order kinetic curve (h) (the inset represents the pseudo-second-order rate constant of OTC degradation).

concentrations at the initial stage of the reaction, but then the degradation rate continued to increase, reaching the maximum of 88.17% at 60 min of the reaction. When the initial OTC concentration is 20–80 mg/L, the degradation efficiency of OTC can reach more than 80% after 60 min, indicating that the system is capable of degrading OTC in a wide concentration range, suggesting that the Fe/Ni1@PNBC is stable over a wide range of OTC concentrations. Furthermore, the degradation rate of OTC reduces with increasing initial concentration, as evidenced by a comparison of the pseudo-second-order rate constant (K_{app}) comparing different treatments. This is because the production of ROS is limited at a fixed PMS dose in the reaction system. When the OTC concentration is too high, more target substances compete with ROS, and OTC molecules cannot be completely degraded.

In order to further analyze the reaction rates of OTC at different initial concentrations, the OTC degradation curves were fitted by zero-order, quasi-first-order and quasi-second-order kinetic models, and the fitting results show that OTC degradation conforms to the quasi-second-order kinetic model, and the fitting correlation R^2 is higher than the fitting correlation of zero-order and quasi-first-order kinetic models (Fig. 6b). Therefore, the corresponding second-order equation is used to calculate the rate constant, the reaction formula is as follows [Eq. (1)].

$$\frac{1}{C_t} - \frac{1}{C_0} = kt \tag{1}$$

where C_t represents the OTC concentration (mg/L) at time t (min), C_0 represents the initial OTC concentration (mg/L), and k represents the reaction rate.

3.3.2. PMS concentration

Fig. 6c shows the effect of PMS concentration on the degradation rate of OTC in the Fe/Ni1@PNBC/PMS system (the initial OTC concentration was 60 mg/L, the catalyst dosage was 1.0 g/L and without pH adjustment). At the initial step of the reaction, when the initial concentration of PMS was adjusted from 0.5 to 1.0 g/L, the rate of OTC degradation increased considerably. For example, it increased by about 25% in the first 10 min. After 20 min of reaction, the difference of degradation rate between the two treatments gradually decreased, and the difference narrowed to less than 10% at the 60 min. However, it can be seen from the changes of degradation rate and k value that the degradation rate begins to decrease with the increase of PMS concentration to more than 1.5 g/L, and the higher the PMS concentration is, the lower the degradation rate is. When the PMS concentration is 2.5 g/L, the final degradation rate decreases to be basically the same as when the PMS concentration is 0.5 g/L. Overall, the degradation efficiency does not increase with the increase of PMS concentration. The reasons for this phenomenon are as follows: when the dosage of PMS is low, the Fe/Ni1@PNBC can promote PMS to produce a huge quantity of active free radicals with the increase of concentration of PMS. However, when the concentration of PMS increases to a certain extent, additional $HSO_5^{\bullet-}$ will trigger the quenching effect of free radicals, the reaction formulas are as follows [Eqs. (2) and (3)] [34].

$$HSO_5^{\bullet-} + SO_4^{\bullet-} \rightarrow SO_5^{2-} + H^+ + SO_4^{2-} \tag{2}$$

$$HSO_5^{\bullet-} + {}^{\bullet}OH \rightarrow SO_5^{2-} + H_2O \tag{3}$$

3.3.3. Catalyst dosage

Fig. 6d shows the degradation rate curve of OTC in Fe/Ni1@PNBC/PMS system when the dosage of catalyst is 0.5, 1.0, 1.5 and 2.0 g/L (the OTC concentration was 80 mg/L, the PMS concentration was 1.5 g/L and without pH adjustment). This result shows that the degradation rate of OTC continued to increase with the increase of catalyst dosage from 0.5 to 2.0 g/L, and K_{app} values also increased

with the dosage of catalyst. This is because the increase of the catalyst dosage can provide more active sites, thus promote PMS activation, produce more ROS and accelerate the reaction rate [34]. It should also be noted that the increase in the OTC degradation rate at the later stage of the reaction is small when the catalyst dosage is from 1.0 to 2.0 g/L. This may be because when the catalyst dosage exceeds optimal values, the PMS was over activated and excess ROS were generated, which induced mutual scavenging effect between ROS, thereby leading to that the degradation rate of OTC was not noticeable changes [27].

3.3.4. Initial solution pH

One of the most crucial exploration elements that influences the activity of PMS and the performance of catalyst is initial solution pH. The effect of initial solution pH on OTC degradation in the Fe/Ni1@PNBC/PMS system is shown in Fig. 6e (the OTC concentration was 60 mg/L, the catalyst dosage was 1.0 g/L and the PMS concentration was 1.0 g/L). The difference in degradation rate between different pH settings was small in the first 5 min of the reaction, but as the reaction progressed, the variation in degradation rate between different treatments began to expand gradually. The degradation curve ranging from 5 to 60 min showed that the concentration of OTC hardly changed in the reaction systems with pH 5 and 11, while the concentration of OTC continued to decrease in the reaction systems with pH 7, 9 and no pH adjustment (initial pH 6). It was discovered that when the initial solution pH was not changed, the degradation rate of OTC was ideal.

It can also be found from the results in Fig. S2 that except in the system without pH adjustment, the OTC degradation in the systems with different pH values did not agree well with the quasi-second-order kinetic models, which may be related to the pH change of the solution in the reaction process. Therefore, the change of pH in the reaction solution with different initial pH is measured. As shown in Fig. 6f, the pH change curve in each system presents a similar type, that is, in the first 30 min of the reaction, the pH value in each treatment system decreases by about 1.0, and then there is basically no change. Although the pH of the solution has not changed significantly, it can still be considered that the reaction will cause the system to reduce the pH, thereby affecting the reaction rate in this system. This finding is consistent with the results of previous studies [10].

Overall, the reaction system was suitable for milder pH values. The specific reasons were as follows: in acidic environments, there was a large amount of free H^+ that can combine with the reactive free radicals $SO_4^{\bullet-}$ and OH to reduce the degradation rate of OTC [26], and the reaction formula was as follows [Eqs. (4) and (5)]. Secondly, the PMS produced relatively less reactive species at lower pH values because PMS was relatively stable resulting in reducing the reaction between the PMS and the catalyst [27]. Therefore, although the total amount of iron ions in solution was highest with pH 5, the degradation rate of OTC was not ideal (Fig. S3). Under strong alkali conditions, although the reaction of generating active free radicals by PMS will not be hindered, it will promote its conversion to $SO_5^{\bullet-}$, leading to a decrease in the degradation rate [35].

$$SO_4^{\bullet-} + H^+ + e^- = HSO_4^{\bullet-} \quad (4)$$

$$^{\bullet}OH + H^+ + e^- = H_2O \quad (5)$$

3.3.5. Gas atmosphere

Under the optimal conditions (the OTC concentration was 60 mg/L, the catalyst dosage was 1.0 g/L, the PMS concentration was 1.0 g/L and without pH adjustment), different gases were introduced into the system to explore the effect of dissolved oxygen on the degradation of OTC by Fe/Ni1@PNBC activated PMS (Fig. 6g and h). When O_2 was introduced into the system, the degradation efficiency of OTC reached 89.88%, which was slightly higher than that in air, and the reaction rate constant was not significantly different from that in air environment. When N_2 was introduced into the system, the degradation efficiency was decreased to 66.03%, and the reaction rate constant was only 0.00062 L/mg·min, which indicated that dissolved oxygen played an important role in the degradation process of OTC. When oxygen was decreased in the system, it was not conducive to the generation and transformation of free radicals, thus affecting the degradation of OTC.

3.3.6. Inorganic anions

There are many anions in natural water, including NO_3^-, Cl^-, CO_3^{2-}, $H_2PO_4^-$ and HCO_3^-, etc. Therefore, it is necessary to design experiments to explore the influence of anions in the reaction system (the OTC concentration was 40 mg/L, the catalyst dosage was 1.0 g/L, the PMS concentration was 1.0 g/L and without pH adjustment). It can be seen from Fig. 7a that NO_3^- in the range of 20~60 mmol/L has a slight inhibitory effect on OTC degradation in the system, which may be because NO_3^- reacted with $SO_4^{\bullet-}$ and OH radicals [Eqs. (6) and (7)] [36]. Fig. 7b showed that Cl^- also had a certain inhibitory effect on OTC degradation, which was mainly reflected in the later stage of the reaction. The inhibition was more severe with increasing concentration of Cl^-. In the presence of Cl^- at a concentration of 60 mmol/L, the degradation rate decreased by about 16% compared with the treatment without Cl^- within 60 min. Because Cl^- will react with free radicals to produce Cl and $Cl_2^{\bullet-}$, but the activities of Cl and $Cl_2^{\bullet-}$ are lower than $SO_4^{\bullet-}$ and OH, so the reaction degradation rate reduced [Eqs. (8) and (9)] [37].

It can be seen from Fig. 7c and d that in the existence of different amounts of CO_3^{2-} and HCO_3^-, the curve and K_{app} values for OTC degradation showed almost the same change rule. At the end of the reaction, the two ions inhibited about 20% of OTC degradation compared with the control, which is because CO_3^{2-} and HCO_3^- can react with $SO_4^{\bullet-}$ and OH [Eqs. (10)–(13)] [27]. Moreover, the presence of $H_2PO_4^-$ in the reaction system significantly limited the degradation of OTC, with the inhibition increasing from 20% within 5 min to 27% within 60 min (Fig. 7e). However, this inhibition degree does not seem to be related to the increase of $H_2PO_4^-$ concentration. The reasons for this phenomenon are $H_2PO_4^-$ reacts with $SO_4^{\bullet-}$ then produces PO_4^{2-} [Eq. (14)] [38]. At the same time, the inhibition of CO_3^{2-}, HCO_3^- and $H_2PO_4^-$ may also be due to the influence of pH. The three ions can be hydrolyzed

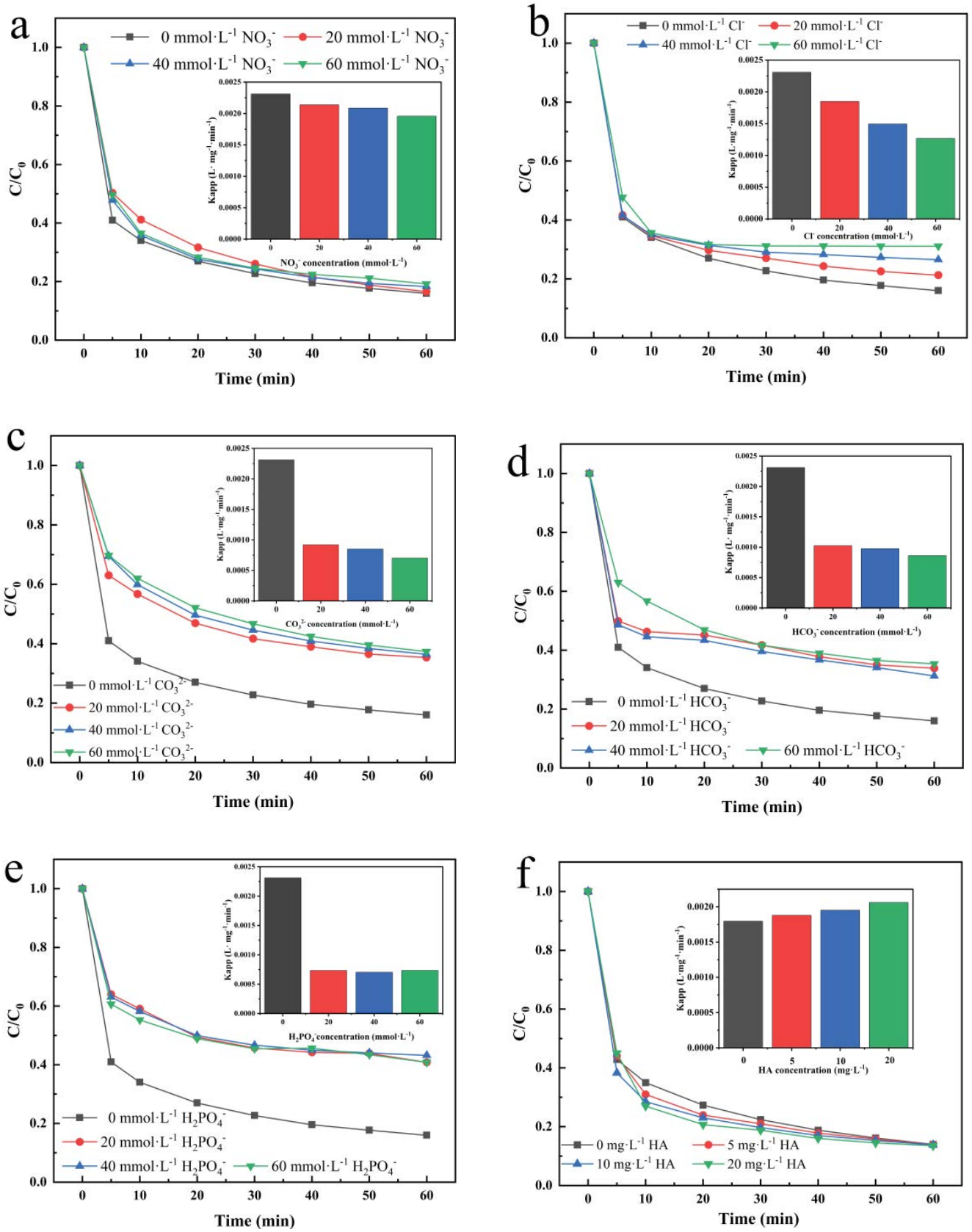

Fig. 7. Effect of inorganic anions NO_3^- (a), Cl^- (b), CO_3^{2-}, (c) HCO_3^-, (d), $H_2PO_4^-$, (e) and humic acid (f) at different concentrations on the OTC degradation (the inset represents the pseudo-second-order rate constant of OTC degradation).

to increase the pH of the system and inhibit the reaction. In conclusion, all anions inhibited the reaction system.

$$^{\bullet}OH + NO_3^- \rightarrow OH^- + NO_3^{\bullet} \quad (6)$$

$$SO_4^{\bullet-} + NO_3^- \rightarrow NO_3^{\bullet} + SO_4^{2-} \quad (7)$$

$$SO_4^{\bullet-} + Cl^- \rightarrow Cl^{\bullet} + SO_4^{2-} \quad (8)$$

$$SO_4^{\bullet-} + 2Cl^- \rightarrow {}^{\bullet}Cl_2 + SO_4^{2-} \quad (9)$$

$$CO_3^{2-} + SO_4^{\bullet-} \rightarrow CO_3^{\bullet-} + SO_4^{2-} \quad (10)$$

$$CO_3^{2-} + {}^{\bullet}OH \rightarrow CO_3^{\bullet-} + OH^- \quad (11)$$

$$HCO_3^- + SO_4^{\bullet-} \rightarrow HCO_3^{\bullet-} + SO_4^{2-} \quad (12)$$

$$HCO_3^- + {}^{\bullet}OH \rightarrow CO_3^{\bullet-} + H_2O \quad (13)$$

$$H_2PO_4^- + SO_4^{\bullet-} \rightarrow PO_4^{\bullet 2-} + H_2SO_4 \quad (14)$$

3.3.7. Humic acid

Dissolved organic substances also exist in natural water, so the experiment explored the effect of HA on degradation capacity of the reaction system (the OTC concentration was 60 mg/L, the catalyst dosage was 1.0 g/L, PMS concentration was 1.0 g/L and without pH adjustment). As shown in Fig. 7f, at the beginning of the reaction, the system adding HA promoted the degradation rate by about 10% compared with the control, but after 40 min, the difference between the treatment adding HA and the control gradually narrowed. In addition, the degradation rate was similar between different HA concentrations, and further increasing HA concentration would not significantly improve the promotion effect of degradation rate. The reason for this phenomenon is that when the HA concentration is low, it could activate PMS which is propitious to the degradation of OTC. While as the HA concentration increases, it competes with OTC for PMS and reduces the effective degradation of OTC. Thus, it may be possible to set the appropriate HA addition to take advantage of the activation of PMS and facilitate the removal of organic pollutants [39].

3.3.8. Degradation efficiency of other pollutants

To further explore the catalytic performance of Fe/Ni1@PNBC for other pollutants, the catalyst was used to activate PMS to degrade methyl blue (MB) (5, 10, 15 and 20 mg/L), methyl orange (MO) (20, 30, 40 and 50 mg/L) and tetracycline (TC) (10, 20, 40 and 60 mg/L) at different concentrations (the catalyst dosage was 1.0 g/L, the PMS concentration was 1.0 g/L and without pH adjustment). After 60 min of reaction, the degradation efficiency of MB, MO and TC was between 83.47%–91.49%, 77.37%–90.87% and 78.94%–91.12%, respectively (Fig. S4). The highest degradation rate for various pollutants can reach more than 90%, indicating that Fe/Ni1@PNBC/PMS system could degrade not only OTC, but also other types of pollutants, which is suitable for the treatment of complex polluted water.

3.4. Reactive species identification and mechanism of PMS activation

3.4.1. Free radical quenching experiment

To resolve the reactive mechanism and determine the ROS leading the reaction, the free radical quenching experiments were carried out (the OTC concentration was 60 mg/L, the catalyst dosage was 1.0 g/L, PMS concentration was 1.0 g/L and without pH adjustment). In the experiments, FFA is the quencher of $^1O_2$ ($K = 1.2 \times 10^8$ M/S), and p-BQ is the quencher of $O_2^{\bullet-}$ ($K = 0.9–1 \times 10^9$ M/S). Moreover, EtOH was used to quench OH ($K = 1.2–2.8 \times 10^9$ M/S) and $SO_4^{\bullet-}$ ($K = 1.6–7.7 \times 10^7$ M/S), and TBA was used to quench OH ($K = 3.8–7.6 \times 10^8$ M/S) [40]. As illustrated in Fig. 8a, in the absence of free radical quencher, the degradation rate of OTC was as high as 90.16%. However, the addition of quenchers reduced the efficiency of OTC degradation to varied degrees, demonstrating that these four free radicals were present in the system and all played a part in OTC degradation. It was worth mentioning that after adding FFA and p-BQ (10 mmol/L), the degradation efficiency of OTC decreased to 51.72% and 53.93%, respectively, the K_{app} values also decreased significantly, indicating that $^1O_2$ and $O_2^{\bullet-}$ acted as a significant role in the degradation process OTC in the system. In contrast, when 30 mmol/L EtOH and TBA were added to the system, the degradation efficiency and K_{app} values decreased less, indicating that OH and $SO_4^{\bullet-}$ contributed little to the degradation process of OTC, and $^1O_2$ and $O_2^{\bullet-}$ were the dominant ROS in Fe/Ni1@PNBC/PMS system.

3.4.2. EPR experiments

In order to further examine the ROS generated in the reaction system, EPR experiments were carried out using DMPO and TEMP as trapping agents. The TEMP was utilized to trap $^1O_2$, while the DMPO was applied to trap $O_2^{\bullet-}$, $SO_4^{\bullet-}$ and OH. The EPR signals included two moments at 1 and 5 min. As the Fig. 8b shows, the EPR typical signals of DMPO-$^{\bullet}$OH with 1:2:2:1 peaks and DMPO-$SO_4^{\bullet-}$ adducts with the 1:1:1:1:1:1 peaks, where the strong signals stand for OH and the relatively weak signals mean $SO_4^{\bullet-}$. Fig. 8c indicates EPR spectral of $O_2^{\bullet-}$, which exhibited characteristic peaks with an intensity ratio of 1:1:1:1. Moreover, in Fig. 8d, the EPR spectral of $^1O_2$ with an intensity ratio of 1:1:1 can be observed. Meanwhile, the intensity of peaks of $O_2^{\bullet-}$, $^1O_2$, OH and $SO_4^{\bullet-}$ were stronger at 5 min than at 1 min, which indicates that these ROS were being generated and involved in the reaction as time passed. The results of EPR experiments were in line with the quenching experiments, which illustrated the essential role of the Fe/Ni1@PNBC in promoting the generation of ROS.

3.4.3. Mechanism of PMS activation by Fe/Ni1@PNBC

Through combining the results of XPS, the valence state of iron and nickel has been determined. For the generation of ROS in Fe/Ni1@PNBC/PMS system, the following mechanism are proposed (Fig. 9). According to the literature [41], Fe(III) can activate PMS to produce Fe(II) and SO_5^-, while Fe(II) can also be oxidized by HSO_5^- to Fe(III)

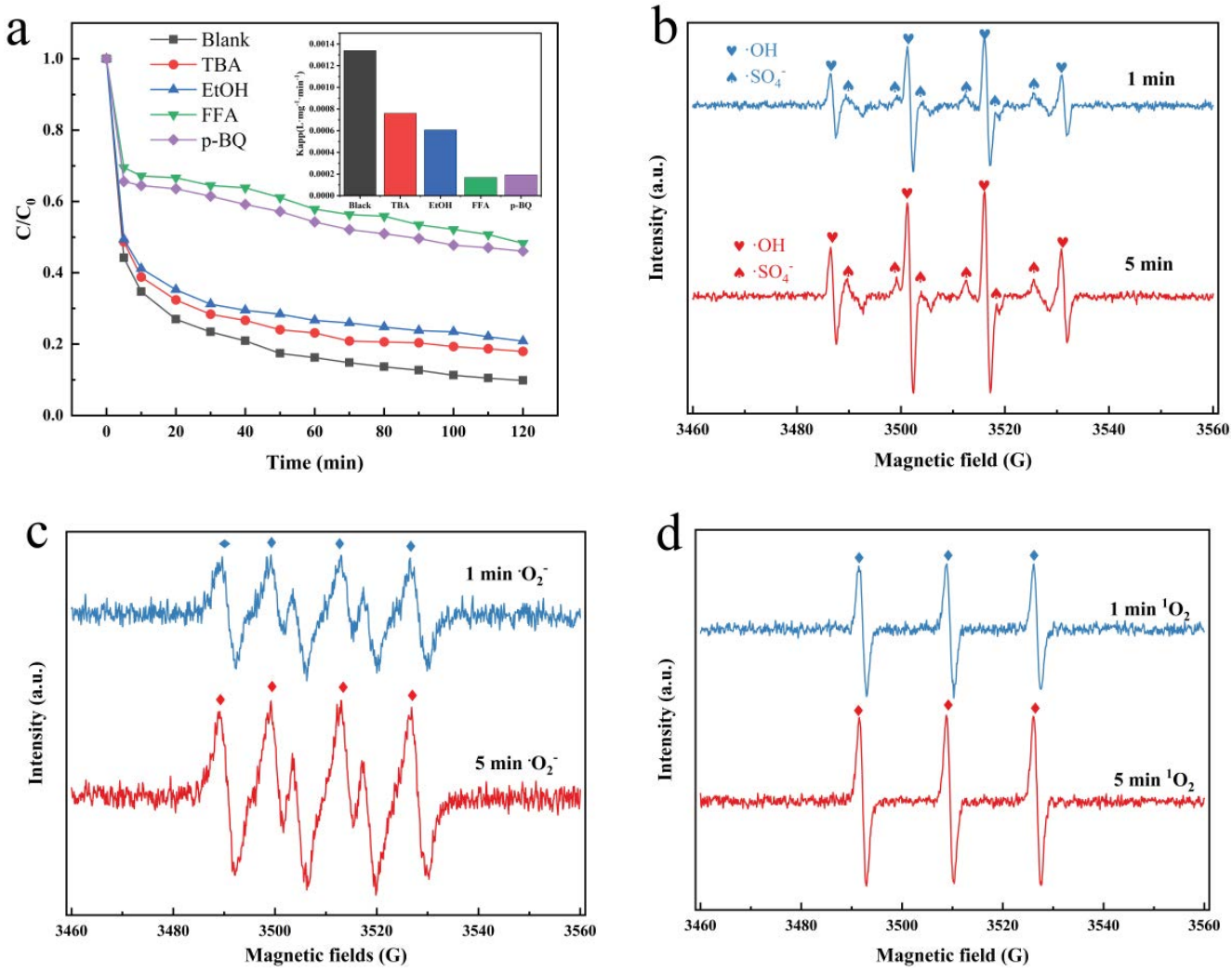

Fig. 8. Effect of free radical quencher on the OTC degradation (a), and EPR spectra of $SO_4^{\bullet-}$, OH (b), O_2^- (c) and $^1O_2$ (d).

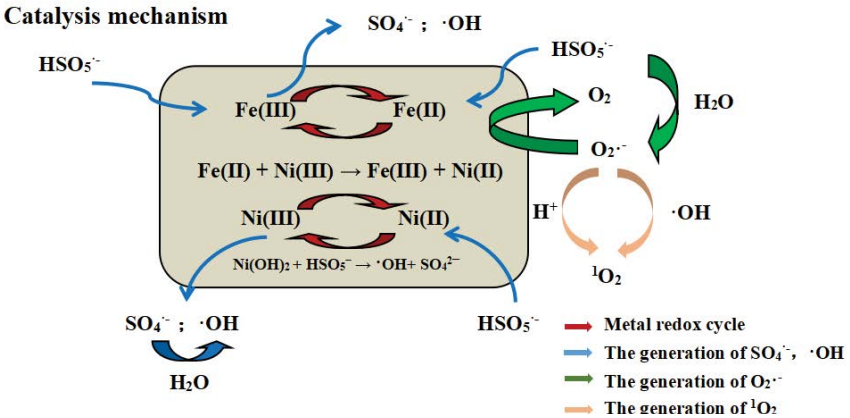

Fig. 9. Generation mechanism of ROS in Fe/Ni1@PNBC/PMS system.

to obtain OH or $SO_4^{\bullet-}$, realizing the redox cycle between Fe(III) and Fe(II) [Eqs. (15)–(17)]. Similarly, there is a redox cycle between Ni(II) and Ni(III), generating OH and $SO_4^{\bullet-}$ [Eqs. (18)–(20)] [25]. Noteworthy, for $Ni(OH)_2$ in the Fe/Ni1@PNBC, its main function is to produce SO_4^{2-} and OH by cleaving the O–O bond in the PMS, which could be the reason for the decrease of nickel content based on the XPS spectrum of Ni2p [Eq. (21)] [42]. Moreover, Fe(II) can react

with Ni(III) to form Fe(III) and Ni(II) [Eq. (22)] because the redox potential of Fe(III)/Fe(II) (0.77 V) is lower than that of Ni(III)/Ni(II) (1.74 V) [27,43]. The transfer of electrons from Fe(II) to Ni(III) is thermodynamically spontaneous. The redox cycle reaction of Fe(III)/Fe(II) and Ni(III)/Ni(II) realizes the continuous production of $SO_4^{\bullet-}$ and OH and promotes the activation of PMS through electron transfer. At the same time, $SO_4^{\bullet-}$ can react with water in the system to produce OH [Eq. (23)] [41]. For $O_2^{\bullet-}$, two production pathways are proposed, one of which relies on the involvement of metal ions and transforms O_2 into $O_2^{\bullet-}$ [Eq. (24)] [26], which is also the reason for the low degradation rate of OTC in the previous N_2 atmosphere experiment, and the other is the hydrolysis of PMS to generate $O_2^{\bullet-}$ [Eqs. (25)–(29)]. In addition, $O_2^{\bullet-}$ can be converted into $^1O_2$ by reacting with OH or H^+ in solution [Eqs. (30) and (31)] [44]. In conclusion, with the involvement of active substances, OTC can be successfully degraded and mineralized into inorganic substances (H_2O and CO_2) [Eq. (32)].

$$Fe(III) + HSO_5^- \rightarrow Fe(II) + SO_5^{\bullet-} + H^+ \quad (15)$$

$$Fe(II) + HSO_5^- \rightarrow Fe(III) + SO_4^{\bullet-} + OH^- \quad (16)$$

$$Fe(II) + HSO_5^- \rightarrow Fe(III) + {}^\bullet OH + SO_4^{2-} \quad (17)$$

$$Ni(II) + HSO_5^- \rightarrow Ni(III) + {}^\bullet OH + SO_4^{2-} \quad (18)$$

$$Ni(II) + HSO_5^- \rightarrow Ni(III) + SO_4^{\bullet-} + OH^- \quad (19)$$

$$Ni(III) + HSO_5^- \rightarrow Ni(II) + SO_4^{\bullet-} + OH^+ \quad (20)$$

$$Ni(OH)_2 + HSO_5^- \rightarrow {}^\bullet OH + SO_4^{2-} \quad (21)$$

$$Fe(II) + Ni(III) \rightarrow Fe(III) + Ni(II) \quad (22)$$

$$SO_4^{\bullet-} + H_2O \rightarrow SO_4^{2-} + OH + H^+ \quad (23)$$

$$Fe(II) + O_2 \rightarrow Fe(III) + O_2^{\bullet-} \quad (24)$$

$$HSO_5^- + H_2O \rightarrow HSO_4^- + H_2O_2 \quad (25)$$

$$SO_5^{2-} + H_2O \rightarrow SO_4^{2-} + H_2O_2 \quad (26)$$

$$H_2O_2 \rightarrow H^+ + HO_2^{\bullet-} \quad (27)$$

$$H_2O_2 + {}^\bullet OH \rightarrow HO_2^{\bullet-} + H_2O \quad (28)$$

$$HO_2^{\bullet-} \rightarrow H^+ + O_2^{\bullet-} \quad (29)$$

$$O_2^{\bullet-} + {}^\bullet OH \rightarrow {}^1O_2 + OH^- \quad (30)$$

$$2O_2^{\bullet-} + 2H^+ \rightarrow {}^1O_2 + H_2O_2 \quad (31)$$

$$SO_4^{\bullet-} + {}^\bullet OH + {}^1O_2 + O_2^{\bullet-} + OTC \rightarrow \text{intermediate} \rightarrow CO_2 + H_2O \quad (32)$$

3.5. Mineralization of OTC

TOC is an important indicator to evaluate the degradation effect of pollutants and is used to evaluate the degree of mineralization of OTC in this study. The experimental conditions were the best conditions (the OTC concentration was 60 mg/L, the catalyst dosage was 1.0 g/L, PMS concentration was 1.0 g/L and without pH adjustment), and the TOC change during OTC degradation is shown in Fig. 10a. In the first 30 min of the reaction, TOC in the reaction system decreased rapidly by about 35%, then TOC continued to decrease slowly, and the mineralization rate reached nearly 45% at 120 min. The OTC mineralization rate slowed at the later stage of the reaction, which may be caused by the deficiency of oxidants in the reaction system. The above results indicate that OTC was broken down into small molecule organic compounds through ring-opening reactions [45]. Some of the degradation products were eventually mineralized to carbon dioxide and water.

3.6. Reusability of Fe/Ni1@PNBC

In order to explore the stability and reusability of the Fe/Ni1@PNBC in the reaction system, the cycling experiments were carried out (the OTC concentration was 60 mg/L, the Fe/Ni1@PNBC dosage was 1.0 g/L, PMS concentration was 1.0 g/L and without pH adjustment). The catalyst after

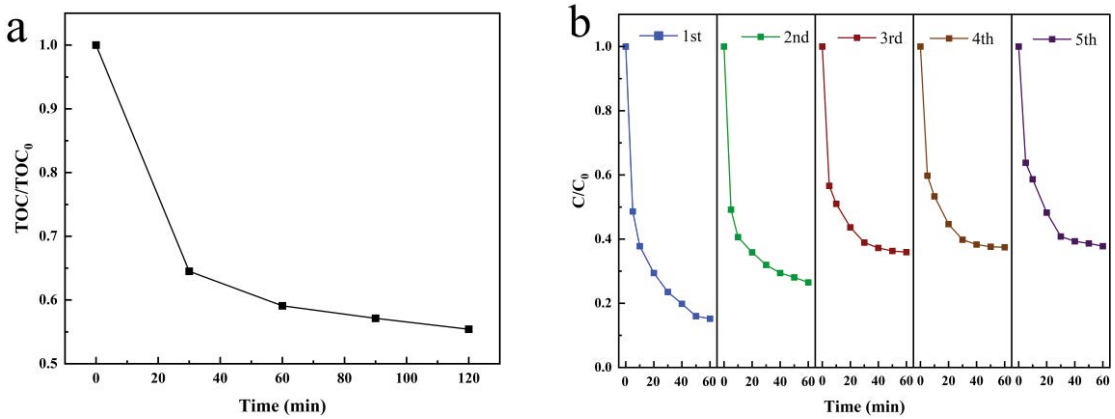

Fig. 10. TOC removal during OTC degradation in Fe/Ni1@PNBC/PMS (a) and reusability of Fe/Ni1@PNBC (b).

60 min of reaction was recovered and cleaned many times using ultrapure water. After the pH had reached neutral, we dried and weighed the catalyst and repeated the experiment for the next time for a total of 5 times. As illustrated in Fig. 10b, the degradation rate of OTC decreased by about 20% in the third use of the catalyst, but the degradation rate was basically stable in the last two degradation experiments. The reduction in catalytic efficiency of the catalyst may be caused by the following factors: (1) the residual OTC on the surface of Fe/Ni1@PNBC prevented the catalyst from interacting with PMS; (2) various products produced in the process of OTC degradation remain on the surface of the catalyst, which was not conducive to the reaction; (3) during the cleaning and drying process, Fe or Ni may be lost in the Fe/Ni1@PNBC [46]. The results showed that Fe/Ni1@PNBC had good reusability and relative stability in the PMS activation for the treatment of antibiotic wastewater.

4. Conclusions

In summary, in this experiment, a pine needle biochar-based catalyst loaded with Fe and Ni was successfully prepared using the impregnation–co-precipitation method. From the characterization results, the catalyst has excellent surface properties as well as great stability. In the degradation experiment, the degradation rate of OTC by the prepared Fe/Ni1@PNBC in the presence of PMS could reach more than 90% under optimal conditions. In addition, through free radical quenching and EPR experiments, the active substances including $^1O_2$, $O_2^{\bullet-}$, OH and $SO_4^{\bullet-}$ in Fe/Ni1@PNBC system were determined, and $^1O_2$ and $O_2^{\bullet-}$ played a major role. And the degradation mechanism of OTC in this system is proposed from the two perspectives which include the redox of metals and the interconversion between the active substances. The catalyst also showed good reusability in the reuse experiment. This experiment provides a foundation for the preparation of heterogeneous catalysts and activation of PMS for the treatment of antibiotic wastewater.

Acknowledgements

This work was supported by National Undergraduate Training Program for Innovation and Entrepreneurship (202110225055).

References

[1] M. Wang, C.Y. Jin, J. Kang, J.Y. Liu, Y.M. Tang, Z.L. Li, S.Y. Li, CuO/g-C_3N_4 2D/2D heterojunction photocatalysts as efficient peroxymonosulfate activators under visible light for oxytetracycline degradation: characterization, efficiency and mechanism, Chem. Eng. J., 416 (2021) 128118, doi: 10.1016/j.cej.2020.128118.

[2] Z.L. Li, M. Wang, C.Y. Jin, J. Kang, J. Liu, H.R. Yang, Y.Q. Zhang, Q.Y. Pu, Y. Zhao, M.Y. You, Synthesis of novel Co_3O_4 hierarchical porous nanosheets via corn stem and MOF-Co templates for efficient oxytetracycline degradation by peroxymonosulfate activation, Chem. Eng. J., 392 (2020) 123789, doi: 10.1016/j.cej.2019.123789.

[3] Y.W. Tang, J. Kang, M. Wang, C.Y. Jin, J.Y. Liu, M. Li, S.Y. Li, Z.L. Li, Catalytic degradation of oxytetracycline via $FeVO_4$ nanorods activating PMS and the insights into the performance and mechanism, J. Environ. Chem. Eng., 9 (2021) 105864, doi: 10.1016/j.jece.2021.105864.

[4] S.V. Manjunath, R.S. Baghel, M. Kumar, Antagonistic and synergistic analysis of antibiotic adsorption on *Prosopis juliflora* activated carbon in multicomponent systems, Chem. Eng. J., 381 (2020) 122713, doi: 10.1016/j.cej.2019.122713.

[5] Z. Li, Y.Q. Sun, Y. Yang, Y.T. Han, T.S. Wang, J.W. Chen, D.C.W. Tsang, Comparing biochar- and bentonite-supported Fe-based catalysts for selective degradation of antibiotics: mechanisms and pathway, Environ. Res., 183 (2020) 109156, doi: 10.1016/j.envres.2020.109156.

[6] Q.L. Ma, H.X. Zhang, X.Y. Zhang, B. Li, R.N. Guo, Q.F. Cheng, X.W. Cheng, Synthesis of magnetic CuO/$MnFe_2O_4$ nanocompisite and its high activity for degradation of levofloxacin by activation of persulfate, Chem. Eng. J., 360 (2019) 848–860.

[7] Y. Gao, Q. Wang, G.Z. Ji, A.M. Li, Degradation of antibiotic pollutants by persulfate activated with various carbon materials, Chem. Eng. J., 429 (2022) 132387, doi: 10.1016/j.cej.2021.132387.

[8] H.J. Wang, M. Mustafa, G. Yu, M. Ostman, Y. Cheng, Y.J. Wang, M, Tysklind, Oxidation of emerging biocides and antibiotics in wastewater by ozonation and the electro-peroxone process, Chemosphere, 235 (2019) 575–585.

[9] E.M. Cuerda-Correa, M.F. Alexandre-Franco, C. Fernández-González, Advanced oxidation processes for the removal of antibiotics from water. An overview, Water, 12 (2020) 102, doi: 10.3390/w12010102.

[10] L. An, P.F. Xiao, Zero-valent iron/activated carbon microelectrolysis to activate peroxydisulfate for efficient degradation of cholrtetracycline in aqueous solution, RSC Adv., 10 (2020) 19401–19409.

[11] J.Y. Yao, Y. Yu, R.J. Qu, J. Chen, Z.L. Huo, F. Zhu, Z.Y. Wang, Fe-activated peroxymonosulfate enhances the degradation of dibutyl phthalate on ground quartz sand, Environ. Sci. Technol., 54 (2020) 9052–9061.

[12] X.X. Xu, J. Chen, R.J. Qu, Z.Y. Wang, Oxidation of tris(2-chloroethyl) phosphate in aqueous solution by UV-activated peroxymonosulfate: kinetics, water matrix effects, degradation products and reaction pathways, Chemosphere, 285 (2017) 833–843.

[13] J.Y. Yao, X.L. Zeng, Z.Y. Wang, Enhanced degradation performance of sulfisoxazole using peroxymonosulfate activated by copper-cobalt oxides in aqueous solution: kinetic study and products identification, Chem. Eng. J., 330 (2017) 345–354.

[14] P.T. Hong, K. Jitae, T.M. Al Tahtamouni, N.L.M. Tri, H.-H. Kim, K.H. Cho, C. Lee, Novel activation of peroxymonosulfate by biochar derived from rice husk toward oxidation of organic contaminants in wastewater, J. Water Process Eng., 33 (2020) 101037, doi: 10.1016/j.jwpe.2019.101037.

[15] Shad, J. Chen, R.J. Qu, A.A. Dar, M. Bin-Jumah, A.A. Allam, Z.Y. Wang, Degradation of sulfadimethoxine in phosphate buffer solution by UV alone, UV/PMS and UV/H_2O_2: kinetics, degradation products, and reaction pathways, Chem. Eng. J., 398 (2020) 125357, doi: 10.1016/j.cej.2020.125357.

[16] P.F. Xiao, L. An, D.D. Wu. The use of carbon materials in persulfate-based advanced oxidation processes: a review, New Carbon Mater., 35 (2020) 667–683.

[17] Z. Li, S.Q. Luo, Y. Yang, J.W. Chen, Highly efficient degradation of trichloroethylene in groundwater based on peroxymonosulfate activation by bentonite supported Fe/Ni bimetallic nanoparticle, Chemosphere, 216 (2019) 499–506.

[18] Z. Musajan, P.F. Xiao, J. Zhao, S. Han, Q.R. Wang, Preparation of cobalt ferrite nanoparticles and application as peroxymonosulfate activators for the removal of Congo red, Desal. Water Treat., 254 (2022) 274–286.

[19] M.M. Barbooti, H. Su, P. Punamiya, D. Sarkar, Oxytetracycline sorption onto Iraqi montmorillonite, Int. J. Environ. Sci. Technol., 11 (2014) 69–76.

[20] H. Li, Q. Jiang, R.Z. Li, B. Zhang, J.X. Zhang, Y. Zhang, Passivation of lead and cerium in soil facilitated by biochar-supported phosphate-doped ferrihydrite: mechanisms and microbial community evolution, J. Hazard. Mater., 436 (2022) 129090, doi: 10.1016/j.jhazmat.2022.129090.

[21] X.N. Li, Y. Song, M.Y. Jia, F. Wang, Y.R. Bian, X. Jiang, A review of researches on biochar adsorbing organic contaminants and its mechanism, Acta Pedol. Sin., 54 (2017) 1313–1325.

[22] Ouyang, J.C. Yan, L.B. Qian, Y. Chen, L. Han, A.Q. Su, W.Y. Zhang, H. Ni, M.F. Chen, Degradation of 1,4-dioxane by biochar supported nano magnetite particles activating persulfate, Chemosphere, 184 (2017) 609–617.
[23] M.J. Xu, H.Y. Zhou, Z.L. Wu, N.W. Li, Z.K. Xiong, G. Yao, B. Lai, Efficient degradation of sulfamethoxazole by $NiCo_2O_4$ modified expanded graphite activated peroxymonosulfate: characterization, mechanism and degradation intermediates, J. Hazard. Mater., 399 (2020) 123103, doi: 10.1016/j.jhazmat.2020.123103.
[24] H. Zheng, J.G. Bao, Y. Huang, L.J. Xiang, Faheem, B.X. Ren, J.K. Du, M.N. Nadagouda, D.D. Dionysiou, Efficient degradation of atrazine with porous sulfurized Fe_2O_3 as catalyst for peroxymonosulfate activation, Appl. Catal., B, 259 (2019) 118056, doi: 10.1016/j.apcatb.2019.118056.
[25] R. Ramachandran, T. Sakthivel, M.Z. Li, H.Q. Shan, Z.X. Xu, F. Wang, Efficient degradation of organic dye using Ni-MOF derived NiCo-LDH as peroxymonosulfate activator, Chemosphere, 271 (2021) 128509, doi: 10.1016/j.chemosphere.2020.128509.
[26] Q.R. Wang, Y.X. Shi, S.Y. Lv, Y. Liang, P.F. Xiao, Peroxymonosulfate activation by tea residue biochar loaded with Fe_3O_4 for the degradation of tetracycline hydrochloride: performance and reaction mechanism, RSC Adv., 11 (2021) 18525–18538.
[27] J. Zhao, P.F. Xiao, S. Han, M. Zulhumar, D.D. Wu, Preparation of magnetic copper ferrite nanoparticle as peroxymonosulfate activating catalyst for effective degradation of levofloxacin, Water Sci. Technol., 85 (2022) 645–663.
[28] J. Liu, Z.W. Zhao, P.H. Shao, F.Y. Cui, Activation of peroxymonosulfate with magnetic Fe_3O_4-MnO_2 core-shell nanocomposites for 4-chlorophenol degradation, Chem. Eng. J., 262 (2015) 854–861.
[29] M. Alhamd, T. Tabatabaie, I. Parseh, F. Amiri, N. Mengelizadeh, Magnetic $CuNiFe_2O_4$ nanoparticles loaded on multi-walled carbon nanotubes as a novel catalyst for peroxymonosulfate activation and degradation of reactive black 5, Environ. Sci. Pollut. Res., 28 (2021) 57099–57114.
[30] B. Wang, S.F. Li, H.B. Wang, S.H. Yao, Insight into the performance and mechanism of magnetic $Ni_{0.5}Cu_{0.5}Fe_2O_4$ in activating peroxydisulfate for ciprofloxacin degradation, Water Sci. Technol., 85 (2022) 1235–1249.
[31] Z.M. Ni, W.H. Yu, L.G. Wang, Z.Q. Guo, Z.H. Ge, Synthesis, characterization and nox absorption capability of Cu-Co-Al hydrotalcite-like compounds, J. Chem. Eng. Chin. Univ., 9 (2005) 223–227.
[32] J. Zhang, Y.F. Xu, G.G. Qian, Z.P. Xu, C. Chen, Q. Liu, Reinvestigation of dehydration and dehydroxylation of hydrotalcite-like compounds through combined TG-DTA-MS analyses, J. Phys. Chem. C, 114 (2010) 10768–10774.
[33] J.M. Bouzaid, R.L. Frost, W.N. Martens, Thermal decomposition of the composite hydrotalcites of iowaite and woodallite, J. Therm. Anal. Calorim., 89 (2007) 511–519.
[34] J. Lu, Y. Zhou, Y.B. Zhou, Efficiently activate peroxymonosulfate by Fe_3O_4@MoS_2 for rapid degradation of sulfonamides, Chem. Eng. J., 422 (2021) 130126, doi: 10.1016/j.cej.2021.130126.
[35] H.Y. Zhou, L.D. Lai, Y.J. Wan, Y.L. He, G. Yao, B. Lai, Molybdenum disulfide (MoS_2): a versatile activator of both peroxymonosulfate and persulfate for the degradation of carbamazepine, Chem. Eng. J., 384 (2020) 123264, doi: 10.1016/j.cej.2019.123264.
[36] S.H. Yao, X.J. Chen, M.A. Gomez, X.C. Ma, H.B. Wang, S.Y. Zang, One-step synthesis of zerovalent-iron-biochar composites to activate persulfate for phenol degradation, Water Sci. Technol., 80 (2019) 1851–1860.
[37] Q.F. Wang, Y.S. Shao, N.Y. Gao, W.H. Chu, X. Shen, X. Lu, J.X. Chen, Y.P. Zhu, Degradation kinetics and mechanism of 2,4-Di-tert-butylphenol with UV/persulfate, Chem. Eng. J., 304 (2016) 201–208.
[38] Z.L. Wu, Y.P. Wang, Z.K. Xiong, Z.M. Ao, S.Y. Pu, G. Yao, B. Lai, Core-shell magnetic Fe_3O_4@Zn/Co-ZIFs to activate peroxymonosulfate for highly efficient degradation of carbamazepine, Appl. Catal., B, 277 (2020) 119136, doi: 10.1016/j.apcatb.2020.119136.
[39] Y. Pang, Z. Tong, L. Tang, Y.N. Liu, K. Luo, Effect of humic acid on the degradation of methylene blue by peroxymonosulfate, Open Chem., 16 (2018) 401–406.
[40] Q.F. Zhong, Q.T. Lin, R.L. Huang, H.Y. Fu, X.F. Zhang, H.Y. Luo, R.B. Xiao, Oxidative degradation of tetracycline using persulfate activated by N and Cu codoped biochar, Chem. Eng. J., 380 (2020) 122608, doi: 10.1016/j.cej.2019.122608.
[41] J.Y. Cao, L.D. Lai, B. Lai, G. Yao, X. Chen, L.P. Song, Degradation of tetracycline by peroxymonosulfate activated with zero-valent iron: performance, intermediates, toxicity and mechanism, Chem. Eng. J., 364 (2019) 45–56.
[42] H. Wang, W.W. Xu, X. Chen, Q.H. Yang, C. Shen, B.S. Zhang, Y.C. Lin, J. Sun, L.J. Zhang, Q.J. Zhang, Z.Y. Lu, L. Chen, Transformation from a non-radical to a radical pathway via the amorphization of a $Ni(OH)_2$ catalyst as a peroxymonosulfate activator for the ultrafast degradation of organic pollutants, Nanoscale, 13 (2021) 7700–7708.
[43] M.X. Shen, Z.J. Huang, L.H. Qiu, Z.H. Chen, X.P. Xiao, X.J. Mo, L.H. Cui, Recycling of Fenton sludge containing Ni as an efficient catalyst for tetracycline degradation through peroxymonosulfate activation, J. Cleaner Prod., 268 (2020) 122174, doi: 10.1016/j.jclepro.2020.122174.
[44] Lyu, Y.C. Li, C. Fang, W. Feng, W.T. Sun, Q.H. Zhang, Enhanced peroxymonosulfate activation by $Ni_xCo_{1-x}OOH$ for efficient catalytic oxidation of organic pollutants, Chem. Res. Chin. Univ., 35 (2019) 440–448.
[45] X.H. Liu, Y. Yang, H.P. Li, Z.G. Yang, Y. Fang, Visible light degradation of tetracycline using oxygen-rich titanium dioxide nanosheets decorated by carbon quantum dots, Chem. Eng. J., 408 (2021) 127259, doi: 10.1016/j.cej.2020.127259.
[46] S. Han, P.F. Xiao, L. An, D.D. Wu, Oxidative degradation of tetracycline using peroxymonosulfate activated by cobalt-doped pomelo peel carbon composite, Environ. Sci. Pollut. Res., 29 (2022) 21656–21669.

Supporting information

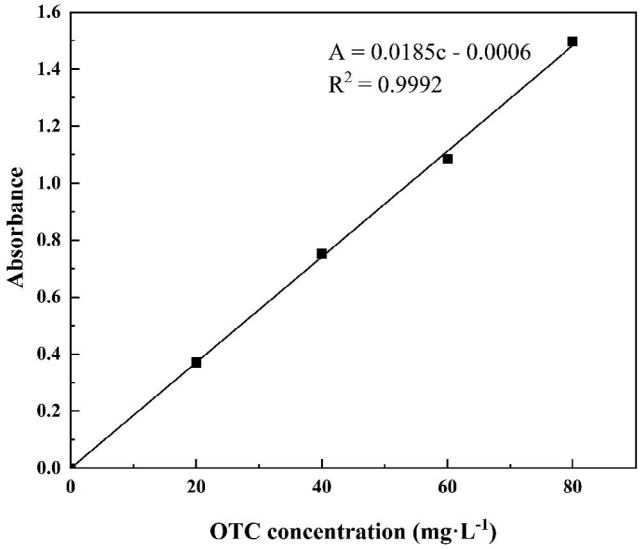

Fig. S1. Standard curve on absorbance vs. OTC concentration.

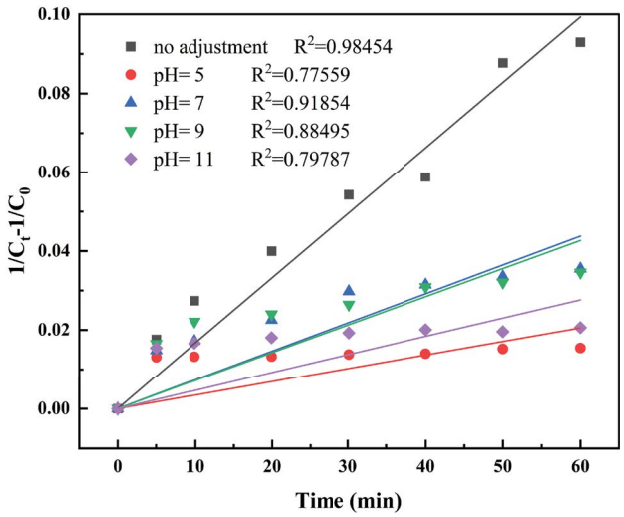

Fig. S2. Model fitting curves of pseudo-second-order rate constants for OTC degradation at different initial pH values.

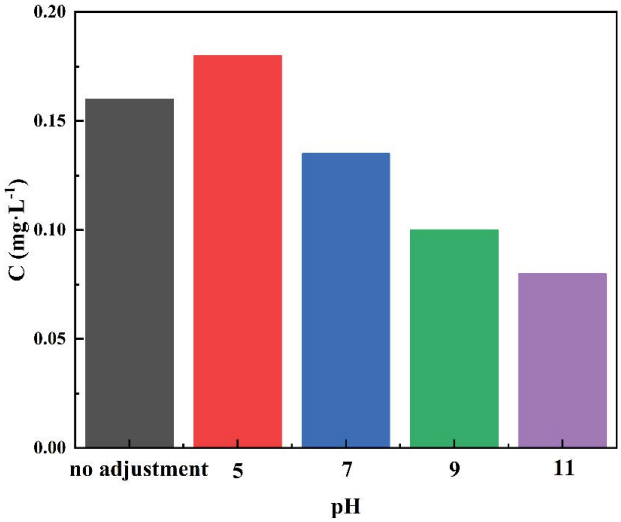

Fig. S3. Total iron content in solution after 60 min of reaction at different initial pH values.

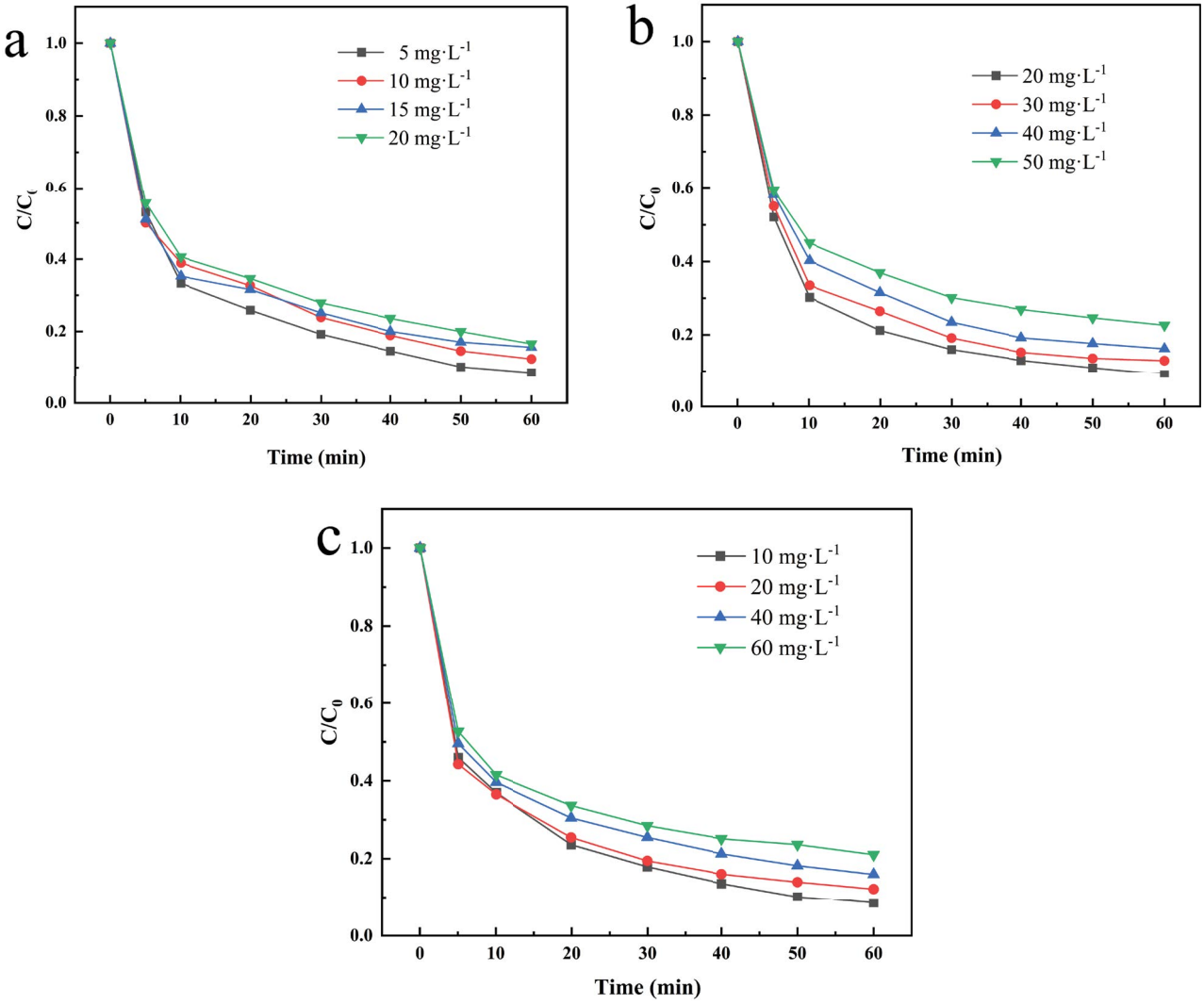

Fig. S4. Degradation of MB (a), MO (b), and TC (c) by PMS activated by Fe/Ni1@PNBC.